Nanotechnology **23** (2012) 385308 (6pp) doi:10.1088/0957-4484/23/38/385308

Fabrication and characterization of solid-state nanopore arrays for high-throughput DNA sequencing

Ruby dela Torre, Joseph Larkin, Alon Singer and Amit Meller

Department of Biomedical Engineering, Department of Physics, Boston University, Boston, MA 02215, USA

E-mail: ameller@bu.edu

Received 16 June 2012, in final form 31 July 2012
Published 5 September 2012
Online at stacks.iop.org/Nano/23/385308

Abstract

We report the fabrication and characterization of uniformly sized nanopore arrays, integrated into an optical detection system for high-throughput DNA sequencing applications. Nanopore arrays were fabricated using focused ion beam milling, followed by TiO_2 coating using atomic layer deposition. The TiO_2 layer decreases the initial pore diameter down to the sub-10 nm range, compatible with the requirements for nanopore-based sequencing using optical readout. We find that the TiO_2 layers produce a lower photoluminescence background as compared with the more widely used Al_2O_3 coatings. The functionality of the nanopore array was demonstrated by the simultaneous optical detection of DNA–quantum dot conjugates, which were electro-kinetically driven through the nanopores. Our optical scheme employs total internal reflection fluorescence microscopy to illuminate a wide area of the TiO_2-coated membrane. A highly parallel system for observing DNA capture events in a uniformly sized 6×6 nanopore array was experimentally realized.

(Some figures may appear in colour only in the online journal)

1. Introduction

Nanopore-based DNA sequencing technologies have recently made significant strides towards a full proof of principles demonstration [1]. In particular, methods that employ the protein channels α-Hemolysin [2, 3] or MspA [4] show great promise due to their ability to distinguish among individual or groups of nucleotides. While protein-based nanopore sequencing may perhaps be the first to reach the commercial market, solid-state nanopores remain extremely attractive due to their superior mechanical stability and scalability [5]. Specifically, optically based DNA sequencing using solid-state nanopores [1, 6, 7] is a viable alternative to protein-based sequencing since it straightforwardly permits parallel detection from many nanopores using high speed cameras.

To enable nucleobase-specific single-molecule fluorescence emission DNA sequencing, we recently introduced an optically based DNA sequencing method, which employs solid-state nanopores [6]. The imaging system comprises total internal reflection fluorescence (TIRF) optics, utilizing wide-field detection of fluorescent molecules on a thin silicon nitride membrane [8]. Essential to this method is the development of a reliable fabrication method for nanopore arrays containing tens to hundreds of pores with diameter ranging between 5–8 nm and pitch at the micrometer scale.

High-resolution transmission electron microscopy (HR-TEM)-based nanopore drilling methodology offers precise control of the pore size and shape. However, the HR-TEM method is not optimized for the fabrication of hundreds of pores in each chip, due to its manual, serial manner. A programmable ion beam system or an electron beam lithography system is more suitable for this application [9–12]. In particular, focused ion beam (FIB) drilling is an attractive platform due to its well-established automation and the small number of process steps required, which minimizes the total fabrication time and obviates the need for etching solutions or etchant gases.

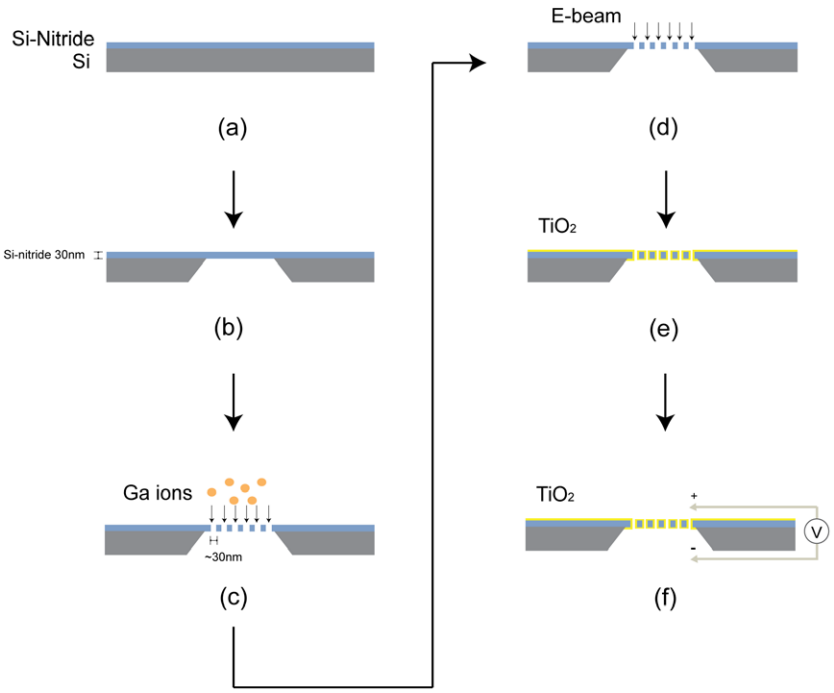

Figure 1. Schematic of the nanopore array fabrication process. A low pressure chemical vapor deposition (LPCVD) process was employed to deposit a low-stress nitride layer above the bulk silicon substrate. A free-standing SiN membrane was fabricated using photolithography. Nanopore arrays were drilled through the SiN membrane using FIB milling. The pore size was measured using TEM. Reduction of the nanopore diameters to sub-10 nm range was achieved using ALD. (a) LPCVD, (b) optical lithography, (c) FIB drilling (d) TEM imaging for pore size determination, (e) atomic layer deposition and (f) electrical test of pore functionality.

Nanopore formation using FIB milling systems has been studied by several groups [9–12], but to date it remains a challenge to reach sub-10 nm pore dimension. Chen *et al* [10] showed that highly circular pores can be drilled using a standard FIB system by depositing Pt during ion beam milling. Li *et al* [13] developed a method of creating nanopores with a custom-built ion beam system. This method permits an ultra-fine sculpturing of sub-5 nm pores; however, it is not optimized for the creation of nanopore arrays since it relies on feedback control of the ion beam from the transmitted ions. Here, we utilized a commercial dual-beam FIB for the fabrication of uniform nanopore arrays that were subsequently reduced in size using atomic layer deposition (ALD) [14–16]. We illustrate the functionality of the method by optically imaging DNA capture events through the nanopore array.

2. Experimental details

The fabrication process we employed to produce nanopore arrays is outlined in figure 1. Silicon nitride (SiN) was deposited onto a silicon substrate using low pressure chemical vapor deposition (LPCVD) to create a low-stress nitride layer. A free-standing 30 nm thick silicon nitride membrane was fabricated using photolithography and subsequent KOH wet etching. An array of nanometer-sized pores was drilled through the silicon nitride membrane using FIB milling (Zeiss NVision 40 Dual-beam FIB-SEM system). The nanopores were drilled while injecting an H_2O precursor for surface charge neutralization. The nanopore diameter was measured using a calibrated TEM (JEOL 2100 TEM).

Reduction of the nanopore diameters to the desired sub-10 nm range was achieved using ALD of TiO_2 (Savannah Cambridge Nanotech S200 ALD). Prior to ALD, the chips were exposed to a UV/ozone stripper to form reactive hydroxylated surfaces to create the essential surface chemistry. The silicon chip was stabilized to the targeted temperature, which in our case was varied from 175 to 300 °C, and to a chamber pressure of 450 mTorr. ALD deposition of TiO_2 involves exposing the chip to a bi-sequential pulsing of H_2O and titanium tetraisopropoxide $Ti[OCH(CH_3)_2]_4$. Water is first pulsed for 20 ms, followed by pulsing of titanium tetraisopropoxide ($Ti[OCH(CH_3)_2]_4$]) (TTIP) for 300 ms. A wait time of 5 s between the water and the TTIP pulse is introduced to ensure that the area of interest is fully saturated with water. This facilitates adsorption of Ti atoms on the surface. Another pulsing of TTIP for 300 ms occurs prior to the next cycle to make certain that the surface reaction is completed. The number of ALD cycles is calculated based on the initial pore size and the deposition rate. The presence of TiO_2 on the SiN membrane was confirmed by XPS measurement, and the final nanopore size and geometry were characterized using a TEM.

3. Results and discussion

We characterized the pore size after FIB milling as a function of dwell time and ion beam current. Our results (shown in figure 2) suggest that at 2 pA ion beam current, the pore diameter is fairly constant at ∼30 nm for dwell times between 60 and 110 ms. It increases by ∼5 nm when the dwell time

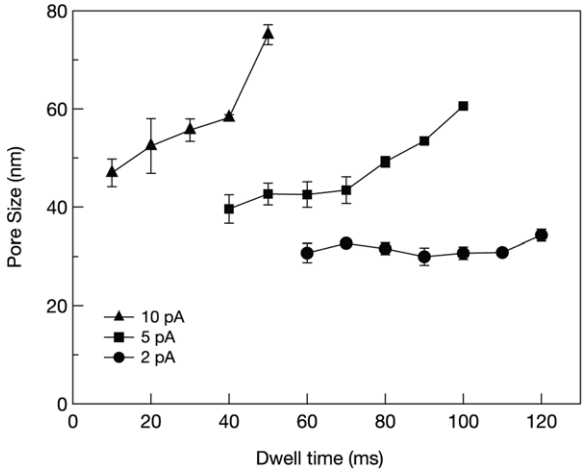

Figure 2. Pore size as a function of FIB dwell time for a 30 nm thick SiN membrane, fabricated at three different probe currents.

is increased to 120 ms. When using ion beam currents of 5 or 10 pA, we observed a steep increase in the pore size as a function of dwell time. At even higher FIB currents, the ion flux resulted in an extremely rapid increase in the pore size for any practical dwell time, thus rendering this regime not useful for our application. The ion beam removes the near-surface atoms from the SiN membrane when its energy is greater than the surface binding energy of the SiN layer [17, 13]. Aside from sputtering, another process which affects the pore size is the lateral mass diffusion of atoms. The diffusion of adatoms causes the pore size to contract, and this can be observed during area scanning after drilling the pore. Scanning of the membrane after a pore is formed can be employed to decrease the pore size. However, surface rippling occurs, presumably due to ion beam roughening/etching followed by relaxation from surface diffusion or viscous flow [18], and thus scanning is not suitable for fine tuning of the pore size due to its low reproducibility and propensity to close the pore completely. To tune the pore size to the sub-10 nm range, our approach is to add layers of TiO_2onto the SiN membrane ALD.

3.1. Atomic layer deposition

While ALD offers atomic-level conformality during deposition, crystalline growth at the nanopore entrance or along its sidewalls changes the contours of the pore. Titanium dioxide deposited at high temperature ALD ($T \geq 250\,^{\circ}\mathrm{C}$) exhibits a crystalline structure. To determine the effect of ALD temperature on the pore shape, the nanopores were imaged before and after ALD, using bright-field high-resolution TEM. At a deposition temperature of 300 °C, the pore shape has a slight deviation from a purely conformal growth due to the crystal orientation of TiO_2 (figure 3). As the number of ALD layers increase, the crystalline structure grown on the membrane surface becomes more pronounced, altering the shape of the pore from a circular (in planar view) to a polygon-shaped pore after ALD. The crystalline structure introduces growth directionality from the nucleation site. At temperatures of 210 and 175 °C, amorphous TiO_2 growth was observed, and the pore shape after ALD was maintained during deposition. At a deposition temperature of 250 °C, the TiO_2 surface is amorphous for thicknesses <15 nm. The conformality and growth rate during ALD are influenced by saturated surface reactions and by diffusion-limited reactions inside the nanopore [19].

Gordon *et al* derived an analytic expression for the time required to coat a pore, t_c, by using a simplified transport-reaction model, wherein a step function approximates the coverage inside the pore and the propagation of the growth front is towards the bottom of the pore [20]. Their model showed that t_c is a function of the aspect ratio AR of the pore, and is given by $t_c = S\frac{\sqrt{2\pi m k_B T}}{p}(1 + \frac{19}{4}(\mathrm{AR}) + \frac{3}{2}(\mathrm{AR})^2)$, where S is the number of absorption sites per unit area, p is the

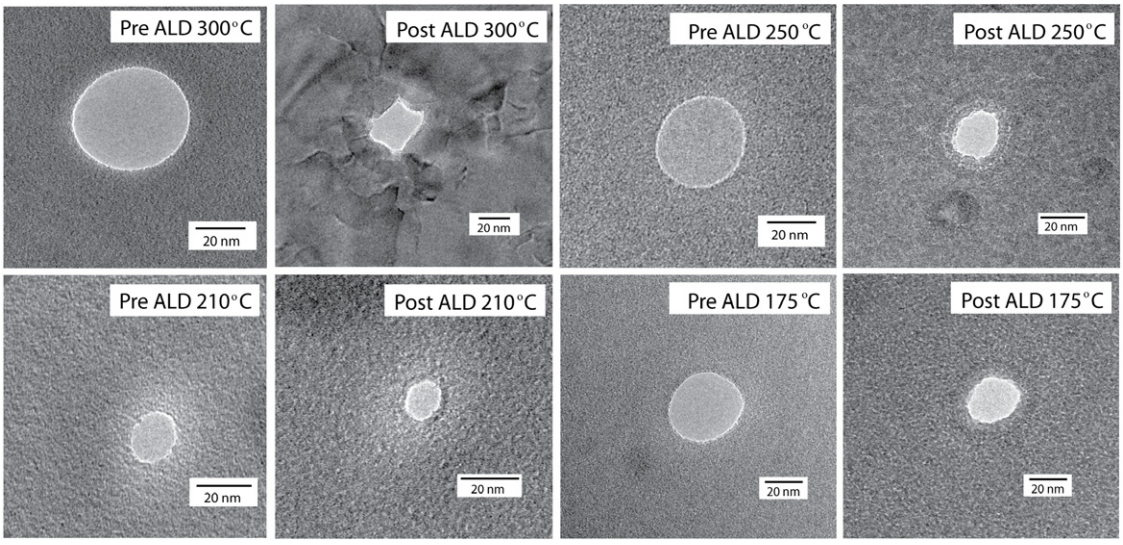

Figure 3. TEM micrographs of FIB-drilled nanopores pre- and post-ALD coating with TiO_2 deposited at different temperatures as indicated.

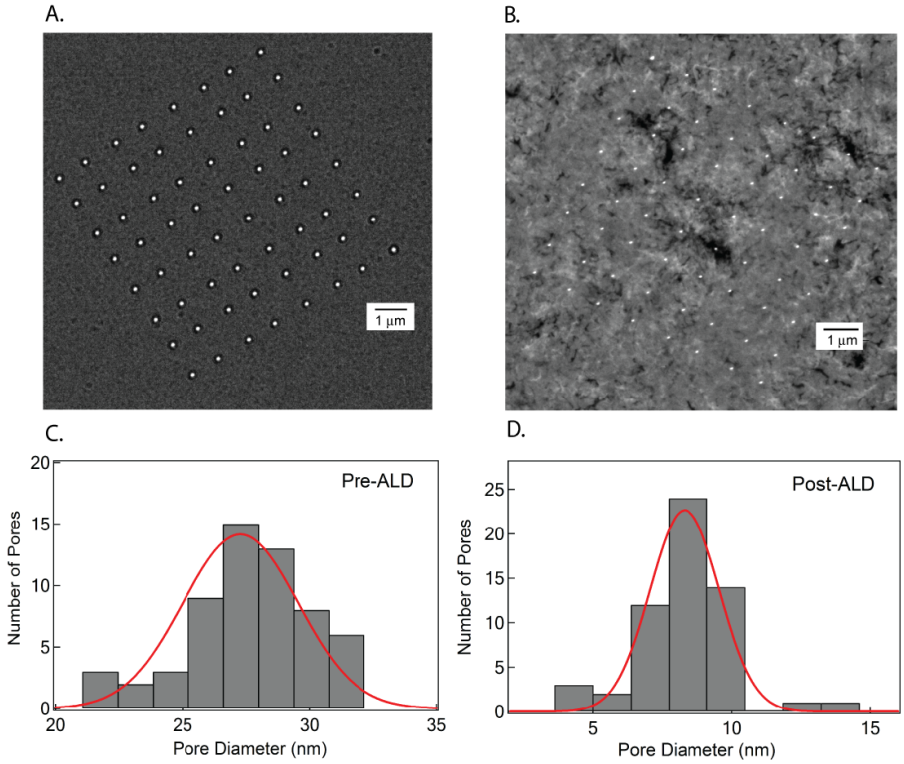

Figure 4. (A) TEM image of an 8 × 8 array of nanopores, fabricated using an FIB current of 2 pA. (B) TEM image of the same membrane post-ALD deposition of TiO_2. The pore size histograms are shown for pre- and post-ALD ((C) and (D), respectively). Solid lines represent Gaussian fits to the distributions.

precursor pressure, m is the mass of the precursor molecule, k_B is the Boltzmann constant and T is the temperature. The time required to saturate a flat surface with the precursor molecules is given by $t = S\frac{\sqrt{2\pi m k_B T}}{p}$. Using the analytic expression above, with AR = 1 (as the membrane thickness in our case is 30 nm and the initial pore diameter is ∼30 nm), the nanopore can be fully coated if the time, t_c, is seven times longer than that for a flat surface of the same material.

The uniformity of the nanopores in an array was characterized by measuring the pore diameter in an 8×8 array. A representative pore size distribution of an 8 × 8 array is shown in figure 4, with 90% of the pores in the array being imaged using a TEM. The average pore diameter before ALD (d_{ave}) is 27.3 nm, with a standard deviation of 3.2 nm, while the average diameter post-ALD (at $T = 210\,^{\circ}C$) is 8.3 nm, with a standard deviation of 1.8 nm. These measurements show that with ALD we have a fine control on the pore dimensions without sacrificing the number of open pores in an array.

3.2. The optical response of TiO_2

The TiO_2 coating maintains the optical transparency of our free-standing membrane. Studies have shown that TiO_2 on multilayer inverse opal has a relatively low luminescence [21, 22]. To investigate whether the ALD-generated TiO_2 is a suitable nanopore coating material for optical detection of single molecules, we conducted optical spectroscopy studies on TiO_2 deposited onto a bare silicon nitride membrane. The photoluminescence spectrum of TiO_2 was obtained using a Raman confocal spectroscopy system (WiTEC Raman confocal microscope with UHTS 300 spectrometer) with an excitation laser emitting at 532 nm. Figure 5(A) shows the photoluminescence spectra for TiO_2-coated membranes processed at different ALD deposition temperatures and for a bare SiN membrane. Our data suggest that TiO_2 has low luminescence in the 580–660 nm region compared to SiN. We surmise that the low photoluminescence effect on TiO_2 film is due to a low occurrence of radiative decay and radiative recombination from the Ti to O energy levels [23], as compared with SiN [24]. The bulk composition of the TiO_2-coated membrane was identified using XPS (x-ray photoelectron spectroscopy), and the spectrum is shown in figure 5(B). A strong peak at the binding energy corresponding to electron ejection from the Ti 2p orbital is observed in the TiO_2-coated sample. The two peaks in the 460 eV region show the electron ejection from the Ti $2p^{3/2}$ and Ti $2p^{1/2}$, and the oxygen peak is at 530 eV. From this XPS spectrum, the stoichiometric film ratio of our ALD deposited TiO_2 is 28.56% Ti and 71.44% O, or Ti:$O_{2.5}$. We attribute the higher than expected level of oxygen to surface oxidation prior to analysis.

Another test was performed to confirm that the TiO_2-coated membrane can be integrated into our optical system. This involved imaging quantum dots, which were immobilized on the TiO_2 membrane using a custom-built TIRF microscope [8]. The TiO_2 membrane was treated with BSA–biotin to facilitate the immobilization of streptavidin-

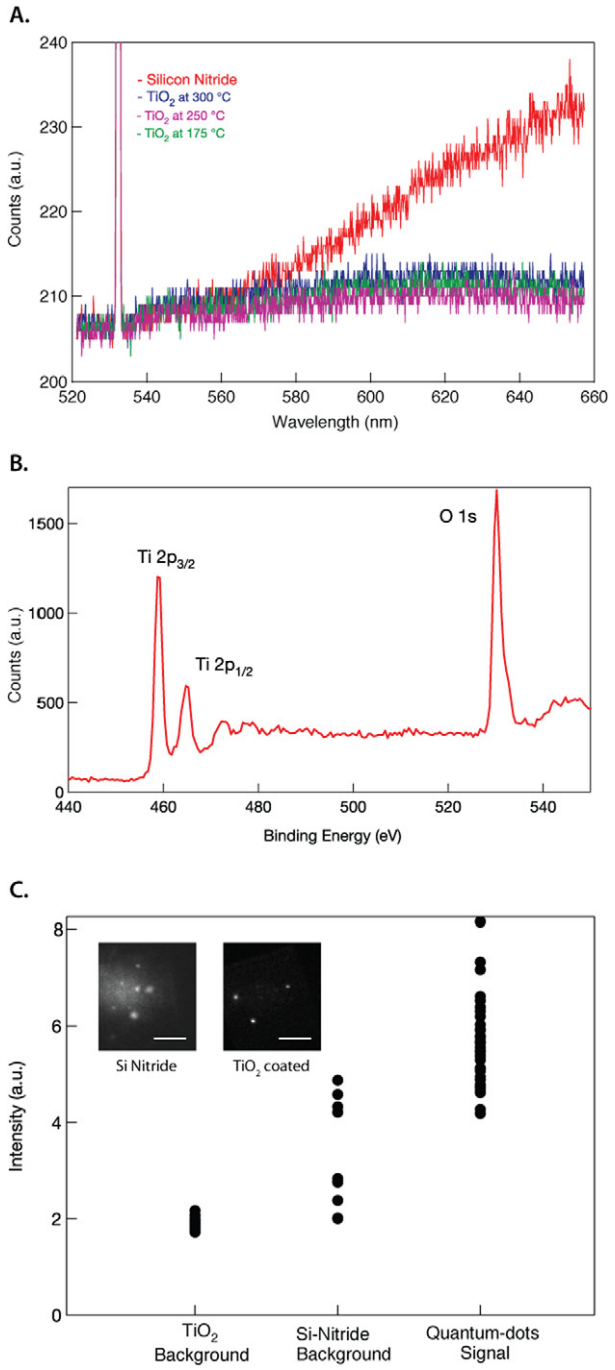

Figure 5. (A) Photoluminescence spectra of TiO_2-coated membranes and a silicon nitride membrane, showing the low photoluminescence at the visible wavelength. (B) XPS spectra of a TiO_2-coated membrane. (C) Optical background comparison between TiO_2 and silicon nitride membranes when excited by a 488 nm laser under TIRF illumination and with the emission band at 650–700 nm. The inset shows the enhancement in image contrast of single quantum dots on a TiO_2-coated membrane versus a silicon nitride membrane (the scale bars equal 5 μm).

conjugated quantum dots (Invitrogen Qdot® 655). The quantum dots were excited using a 488 nm laser (Coherent Sapphire 488) and its emission signal was imaged onto an EMCCD detector (Andor DU-897), with an exposure time of 2 ms. Figure 5(C) shows a comparison of the

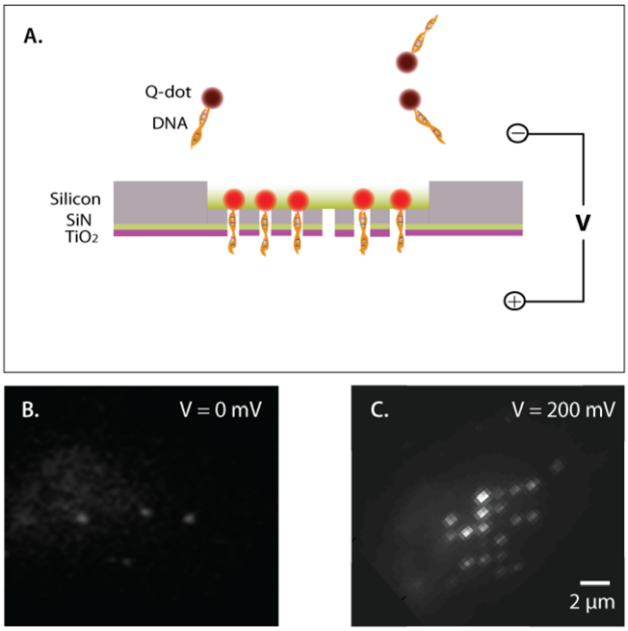

Figure 6. (A) Schematic illustration of the TIRF-based imaging of the nanopore array and Qdot–DNA conjugates. Bottom: optical images of the membrane before (B) and after application of a positive voltage (C). The discrete fluorescent spots arise from the Qdot–DNA conjugates, exhibiting partial occupancy of a 6 × 6 nanopore array when a positive voltage is applied.

optical background at the 650–700 nm wavelength from a TiO_2-coated membrane and from bare silicon nitride. It also plots the optical signal from the quantum dot fluorescence. It can be seen from figure 5(C) that the TiO_2-coated membrane exhibits a three times improvement in the background compared to a bare silicon nitride membrane due to its low luminescence property.

3.3. DNA capture in a nanopore array

To illustrate the functionality of the TiO_2-coated nanopore arrays, we used an objective-based TIRF [8] with a 488 nm laser to image 1 kbp ds-DNA, which was attached to a streptavidin-coated quantum dot. The quantum dot serves as an anchor to hold the DNA inside the nanopore when an electric field is applied. When an external electrical field (V = 200 mV) is applied across the membrane, the Qdot–DNA molecules are randomly drawn towards the nanopores (the concentration of Qdot–DNA molecules in the *cis* chamber is ∼100 pM). In figure 6, we show a representative series of images when the DNA–quantum dot molecules are trapped inside a 6 × 6 nanopore array. The Qdot–DNA molecules are captured in the pore, but they do not translocate through the pore, because the diameter of the quantum dot is larger than the pore diameter. Figure 6(B) shows a CCD image of an illuminated area in the membrane within the vicinity of the nanopore array when no electrical field is present. Since there is no applied voltage, the molecules are freely diffusing in the ionic solution. Upon application of a positive voltage, we observe clear fluorescence signals in 18 pores, indicating the lodging of Qdot–DNA conjugates in each

pore. This implies that 50% of the pores in the 6 × 6 array were occupied by DNA strands during the imaging period and the application of a positive voltage. The locations of the fluorescence spots, imaged by the EMCCD camera, correspond to the locations of the nanopores on the chip. Two adjacent nanopores in this array have a spacing of 1.5 μm. This corresponds well with the spacing between the fluorescence signals from the quantum dots. Moreover, switching off (or reversal) of the electric field resulted in the disappearance of the fluorescence signal, due to the escape of the Qdot–DNA from the nanopores (data not shown).

4. Conclusions

In summary, we have demonstrated that uniformly sized nanopore arrays can be fabricated using FIB drilling and subsequent ALD. A commercial FIB system can be optimized and easily automated to reproducibly create tens to hundreds of pores per chip, whose diameters can be decreased to sub-10 nm using ALD. By employing a simple, direct process for creating nanopores, we address the need for a fabrication method that is applicable to an optical DNA sequencing platform.

Optical detection of DNA molecules conjugated to Qdots was performed using 6 × 6 nanopore arrays. To enhance the detection capability, the nanopores were coated with TiO_2 during ALD, which we have shown to produce less luminescence than silicon nitride in the 580–700 nm region. Furthermore, we optimized the TiO_2 ALD process, such that the nanopore contours remained conformal after layers of TiO_2 were added to obtain a pore size suitable for DNA studies. This type of nanopore array, integrated into an optical system, is a major step towards the realization of a low cost, high-throughput DNA sequencing device.

Acknowledgments

We acknowledge financial support from National Human Genome Research Institute award R01 HG-005871. We acknowledge support from the Center for Nanoscale Systems at Harvard University where parts of the fabrication process were performed.

References

[1] Branton D *et al* 2008 The potential and challenges of nanopore sequencing *Nature Biotechnol.* **26** 1146–53
[2] Clarke J *et al* 2009 Continuous base identification for single-molecule nanopore DNA sequencing *Nature Nanotechnol.* **4** 265–70
[3] Cherf G *et al* 2012 Automated forward and reverse ratcheting of DNA in a nanopore at 5-A precision *Nature Biotechnol.* **30** 344–8
[4] Manrao E *et al* 2012 Reading DNA at single-nucleotide resolution with a mutant MspA nanopore and phi29 DNA polymerase *Nature Biotechnol.* **30** 349–54
[5] Venkatesan B M and Bashir R 2011 Nanopore sensors for nucleic acid analysis *Nature Nanotechnol.* **6** 615–24
[6] McNally B *et al* 2010 Optical recognition of converted DNA nucleotides for single molecule DNA sequencing using nanopore arrays *Nano Lett.* **10** 2237–44
[7] Singer A *et al* 2012 DNA sequencing by nanopore induced photon emission (SNIPE) *Nanopore-Based Technology: Single Molecule Characterization and DNA Sequencing* (New York: Humana Press, Springer)
[8] Soni G *et al* 2010 Synchronous optical and electrical detection of biomolecules traversing through solid-state nanopores. *Rev. Sci. Instrum.* **81** 014301
[9] Kim M-J *et al* 2006 Rapid fabrication of uniform nanopores and nanopore arrays *Adv. Mater.* **18** 3149–53
[10] Chen P *et al* 2009 Fast single-step fabrication of nanopores *Nanotechnology* **20** 015302
[11] Wu M-Y *et al* 2010 TEM study of locally coated nanopore fabricated by ion-beam-induced deposition in a thin membrane *Micron* **41** 609–14
[12] Mussi V *et al* 2010 DNA-functionalized solid-state nanopore for biosensing *Nanotechnology* **21** 145102
[13] Li J *et al* 2001 Ion beam sculpting at nanometer length scales *Nature* **412** 166
[14] Venkatesan B M *et al* 2008 Highly sensitive nanopore sensors for DNA analysis *Adv. Mater.* **21** 2771–6
[15] Nam S W *et al* 2009 Ionic field effect transistors with sub-10 nm multiple nanopores *Nano Lett.* **9** 2044–8
[16] Chen P *et al* 2004 Atomic layer deposition to fine-tune the surface properties and diameters of fabricated nanopores *Nano Lett.* **4** 1333–7
[17] Biersack J P and Eckstein W 1984 Sputtering studies with the Monte Carlo program TRIM.SP *Appl. Phys. Lett.* **34** 73–94
[18] Erlebacher J *et al* 1999 Spontaneous pattern formation on ion bombarded Si(001) *Phys. Rev. Lett.* **82** 2330–3
[19] Elam J W *et al* 2003 Conformal coating on ultrahigh-aspect ratio nanopores of anodic alumina by atomic layer deposition *Chem. Mater.* **15** 3507–17
[20] Gordon R G *et al* 2003 A kinetic model by step coverage by atomic layer deposition in narrow holes or trenches *Chem. Vapor Depos.* **9** 73–8
[21] King J, Graugnard E and Summers C J 2006 Photoluminescence modification by high-order photonic bands in TiO_2/ZnS:Mn multilayer inverse opals *Appl. Phys. Lett.* **88** 1–3
[22] Palik E 1998 *Handbook of Optical Constants of Solids* (San Diego, CA: Academic Press)
[23] Wang X *et al* 2010 Trap states and carrier dynamics of TiO_2 studied by photoluminescence spectroscopy under weak excitation condition *Phys. Chem. Chem. Phys.* **12** 7083–90
[24] Desphande S *et al* 1995 Optical properties of silicon nitride films deposited by hot filament chemical vapor deposition *J. Appl. Phys.* **77** 6535–41